Materials identification using a small-scale pixellated X-ray diffraction system

D O'Flynn[1], C. Crews[1], I. Drakos[1], C. Christodoulou[1], M.D. Wilson[2], M.C. Veale[2], P. Seller[2] and R.D. Speller[1]

[1]Department of Medical Physics and Biomedical Engineering, University College London, WC1E 6BT, United Kingdom
[2]Detector Development Group, Rutherford Appleton Laboratory, Harwell Science & Innovation Campus, Didcot OX11 0QX, United Kingdom

E-mail: d.oflynn@ucl.ac.uk

Abstract. A transmission X-ray diffraction system has been developed using a pixellated, energy-resolving detector (HEXITEC) and a small-scale, mains operated X-ray source (Amptek Mini-X). HEXITEC enables diffraction to be measured without the requirement of incident spectrum filtration, or collimation of the scatter from the sample, preserving a large proportion of the useful signal compared with other diffraction techniques. Due to this efficiency, sufficient molecular information for material identification can be obtained within five seconds despite the relatively low X-ray source power. Diffraction data are presented from caffeine, hexamine, paracetamol, plastic explosives and narcotics. The capability to determine molecular information from aspirin tablets inside their packaging is demonstrated. Material selectivity and the potential for a sample classification model is shown with principal component analysis, through which each different material can be clearly resolved.

1. Introduction

X-ray diffraction (XRD) is a technique which gives detailed information on the molecular structure of a material, arising due to the constructive interference of coherently scattered X-rays from different atomic planes. XRD is a powerful tool for sample identification, giving very high material specificity and sensitivity [1, 2, 3]. A large advantage of XRD over Raman imaging, another molecular fingerprinting technique, is the penetrating nature of X-rays compared with laser light. With transmission XRD, objects can be probed whilst inside packaging, which is of particular use in the cases of suspicious powders or pharmaceuticals, since samples can be kept intact and preparation time is reduced. By comparison with X-ray imaging methods, greater sample sensitivity and specificity can be achieved with XRD due to the molecular information provided. The relation describing the conditions for an increase in observed intensity due to XRD is summarised by Bragg's law: $n\lambda = 2d\sin\theta$, where λ is the X-ray wavelength, θ is the angle between the incident X-rays and the crystallographic planes in the sample and d gives the spacing between these planes.

Standard experimental approaches to XRD can be divided into two broad categories: angular dispersive (ADXRD) and energy dispersive (EDXRD). The former approach requires a close-to-monochromatic X-ray source, and Bragg's law is probed by detecting the X-ray intensity as a function of scattering angle. This can be performed by a mechanical rotation of the X-ray source and detector about the sample, or by the use of a pixellated X-ray detector with an area large enough to capture a sufficient range of angles. With EDXRD, the scattering angle is kept fixed, and diffraction from a broad spectrum of X-ray energies is measured by the use of a single element energy-resolving detector (or an array of detectors) [4]. EDXRD is typically performed in transmission mode (with the detector placed on the opposite side of the sample to the X-ray source), and ADXRD is measured in either reflection or transmission. A lower incident X-ray energy is generally used in reflection geometries (for example, Cu Kα radiation: 8.06 keV), since this gives a wide spread of diffraction angles for a given set of sample d-spacings, making peaks easier to resolve. In transmission, the X-ray energy needs to be greater (of the order of 10-100 keV) in order for photons to pass through the sample; alternatively, the sample thickness needs to be on the sub-millimetre scale.

In order to perform real-world materials identification with XRD, there is a requirement to overcome limitations in efficiency and/or practicality of both angular dispersive and energy dispersive techniques. The need for a rotation of source and detector for ADXRD in diffractometers results in equipment which is large and unwieldy, and scanning inside packaging is not possible with the low X-ray energies used. Transmission ADXRD is limited by the need for a narrow energy window at an energy high enough for reasonable sample penetration - without the use of a synchrotron it is difficult to achieve such a small range of energies - and there is a trade-off between energy resolution and X-ray flux when using spectral filtration methods. EDXRD requires the diffracted beam to be very strongly collimated in order to reduce the broadening of the

diffraction peaks due to low angular resolution. Such collimation means that the vast majority of the diffracted signal is not utilised. Each technique has inherent issues with counting statistics since they discard a lot of useful information from the scattered X-rays - either spatial, spectral, or both. Pixellated diffraction (PixD) is a method of combining transmission ADXRD and EDXRD, utilising the benefits of both approaches - i.e. simultaneous measurements over a range of scattering angles and X-ray energies [5, 6]. PixD was developed with the use of the HEXITEC pixellated energy-resolving detector [7, 8, 9]. HEXITEC is made up of a $20 \times 20 \times 1$ mm cadmium telluride (CdTe) crystal bump bonded to an application-specific integrated circuit (ASIC) to give an 80×80 pixel array with 250 µm pitch. Unlike germanium-based energy resolving detectors, CdTe does not need to be operated at cryogenic temperatures. With HEXITEC, the crystal is peltier cooled, and typical operating temperatures are between 0-10 °C. The ASIC detects the charge created by each photon interaction, and converts this into an energy value. Therefore, each pixel outputs an individual energy spectrum for a single acquisition. This is in contrast to other pixellated, energy-resolving detectors in which a number of energy thresholds (typically four or less) can be set by the user, above which all photon interactions are counted indistinguishably [10, 11, 12, 13, 14]. The energy-resolving capability of HEXITEC allows an unfiltered incident X-ray beam to be used for XRD. The pixellation of the detector means that the angular distribution of the diffracted X-rays can be observed without the need for a collimator positioned between the sample and the detector, provided the incident beam is sufficiently collimated and the sample is thin enough to reduce the uncertainty in the origin of the diffracted X-rays along the incident beam axis [6]. The combination of pixellation and energy resolution gives a greatly enhanced measurable diffraction signal intensity compared with ADXRD and EDXRD. A previous report has demonstrated accurate material specificity with the PixD technique - particularly that of plastic explosive samples - with sufficient counting statistics for identification obtained in one second using a high power (420 W) X-ray source [5].

In moving towards more practical applications of the pixellated diffraction system, this report presents results from performing the PixD technique using a small, lightweight, mains/battery operated X-ray source. The effects of this source on the observed diffraction spectra of a range of materials are discussed, covering plastic explosives, illicit drugs and pharmaceuticals. The potential of the system for classifying materials within packaging is demonstrated for aspirin tablets. This capability is of particular relevance to the pharmaceutical industry, where counterfeiting is a serious global problem [15, 16].

2. Experimental detail

The X-ray source utilised for this study was an Amptek Mini-X, with dimensions of $185 \times 58 \times 47$mm. The Mini-X had an Au target and a maximum tube voltage of 50 kV and power output of 4 W. The X-ray beam was collimated at the source by a 12 mm

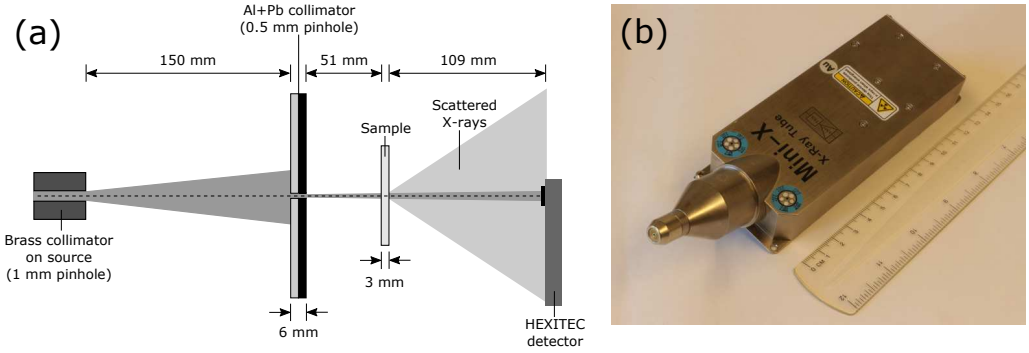

Figure 1. (a) Schematic plan view of the experimental setup (b) The Amptek Mini-X source

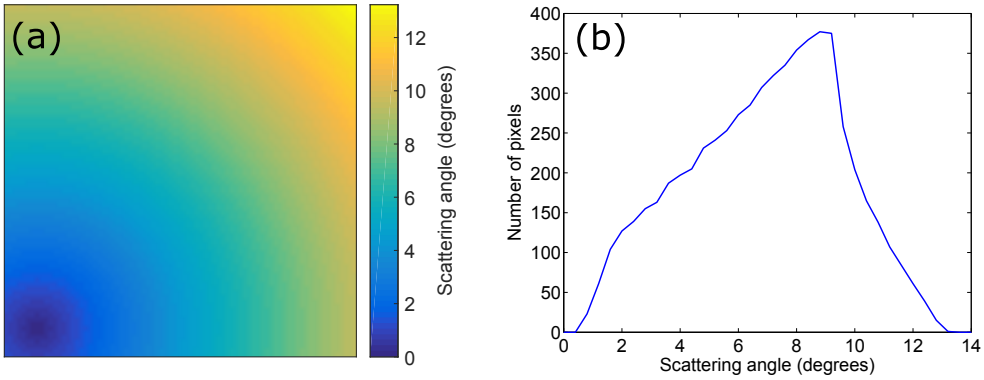

Figure 2. (a) The scattering angles measured by the pixels across the detector, due to sample and detector positioning. (b) The number of pixels which are represented as a function of scattering angle (pixels covered by the beam stop are omitted).

long brass collimator insert with a 1 mm pinhole, and by an additional 0.5 mm lead pinhole before the sample. The HEXITEC detector was placed behind the sample, with the collimated X-ray beam aligned with the bottom-left corner of the detector. A lead beam stop covering the primary beam was put in place during diffraction measurements, and pixels covered by the beam stop were not included in the data analysis. A schematic plan view of the experimental setup and image of the Mini-X source are shown in Figure 1. The source was operated at 50 kV, and the maximum tube current at this voltage of 80 µA. The scattering angle as a function of pixel position across the detector given by this geometry is shown in Figure 2. Due to the radial nature of the diffraction and the positioning of the detector, some scattering angles were sampled more frequently than others (Figure 2 (b)). For example, there are over 6 times the number of pixels positioned at a scattering angle of 9° than at 12°. In combination with the energy spectra of the pixels, this introduced a bias into the overall momentum transfer plot, which was corrected for in the data analysis.

The diffraction profiles of a range of different polycrystalline materials were taken with the small-scale pixellated diffraction setup for this work. For comparison with the large-scale system, caffeine, hexamine and three different explosive materials were

tested. In order to demonstrate the potential of this system for material identification of illicit/counterfeit drugs, diffraction data was also taken for three diamorphine (heroin) and two cocaine samples seized by the UK Border Force, aspirin tablets (Tesco Dispersible Aspirin, 300 mg) and a crushed paracetamol tablet. Diffraction profiles for the aspirin were measured both inside and outside the blister pack to demonstrate the ability of the technique to identify materials without the need to open the packaging. The caffeine, hexamine, paracetamol and explosive samples were each 3 mm thick, and held in place between layers of Mylar film. The drug samples were contained inside clear polythene bags which could not be opened for security reasons; these bags were lightly compressed between two flat plastic plates (with large holes for the incident and diffracted X-rays to pass through unobstructed) to give sample thicknesses of 4 ± 1mm. The aspirin tablets were kept in their standard form, and were 3.5 mm thick.

A common issue with pixellated, energy-resolving detectors is the presence of charge sharing, i.e. when the charge cloud generated in the CdTe from a single photon interaction is spread across more than one detector pixel. This, in turn, causes the energy contribution from the photon to be divided across these pixels. Charge-sharing effects are mitigated in HEXITEC due to the relatively large pixel size, although they remain significant. Charge-sharing discrimination was applied for this work, i.e. when events were detected in neighbouring pixels in the same frame, these events were removed from the final data. The counting rate used was 5520 frames per second.

The spread of X-ray energies up to 50 keV from the Mini-X source defined the momentum transfer range able to be probed in this work (for a given range of angles). The effect of acquisition times on the counting statistics with the maximum X-ray flux of 80 µA was observed by taking multiple diffraction profiles for each sample over a range of times from 1-600 seconds.

3. Results and discussion

3.1. Energy-angle space in pixellated diffraction

The background subtracted pixellated diffraction data for caffeine at three discrete energies, acquired over 600 seconds, are shown in Figure 3. The two arcs visible represent diffraction from four different atomic spacings of caffeine (7.53 Å, 7.40 Å, 3.37 Å and 3.30 Å) - the respective first two and latter two spacings are close enough so as to be unresolvable with this technique. It can be seen that approximately one-quarter of the diffraction "cones" emitted from the sample are intersected by the detector. Moving to higher X-ray energy windows, the arcs gradually decrease in radius - this behaviour is as described by Bragg's law, and is also represented by an energy-angle map in Figure 4.

The pixellated diffraction information was converted into a plot of momentum transfer space utilising the unique energy spectra and scattering angle of each detector

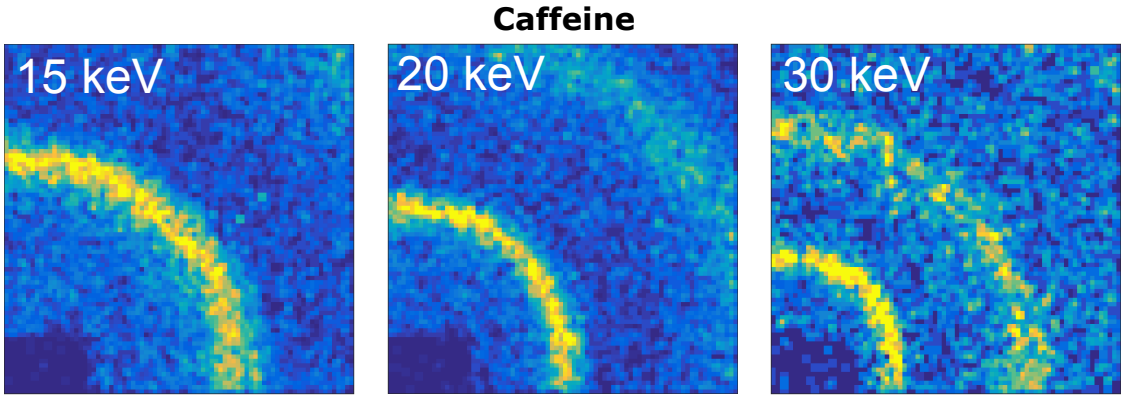

Figure 3. Pixellated X-ray diffraction from caffeine, with X-rays generated at 50 kV and 80 µA, and an acquisition time of 600 s. The energy windows shown have a width of 2 keV. The region of low intensity in the bottom-left corner of the detector is due to the lead beam stop.

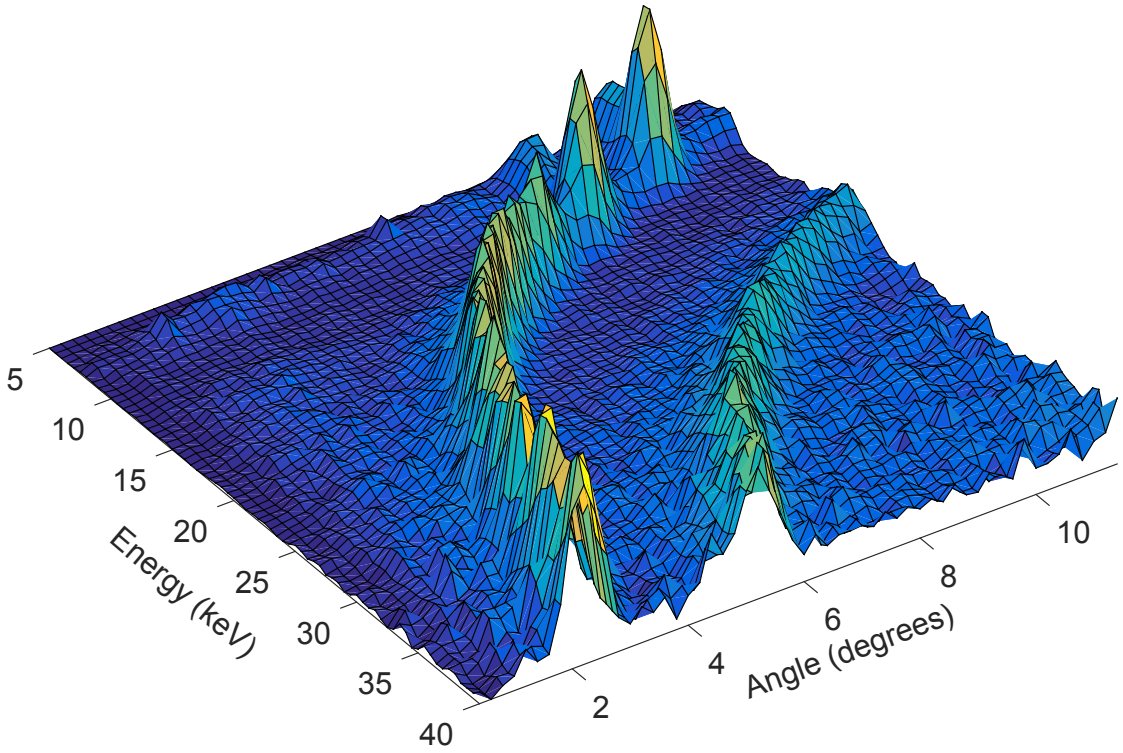

Figure 4. An energy-angle map of the pixellated X-ray diffraction signal from caffeine.

pixel, and the relationship:

$$x = \frac{E}{hc} \sin\theta \tag{1}$$

where x is the momentum transfer for a photon of energy E scattered through an angle 2θ. When the pixel spectra are converted into the generic momentum transfer space, they can be summed together to fully utilise the counting statistics of the diffraction data [5]. The peaks seen at momentum transfer values of 0.68 and 1.48 nm^{-1} (from

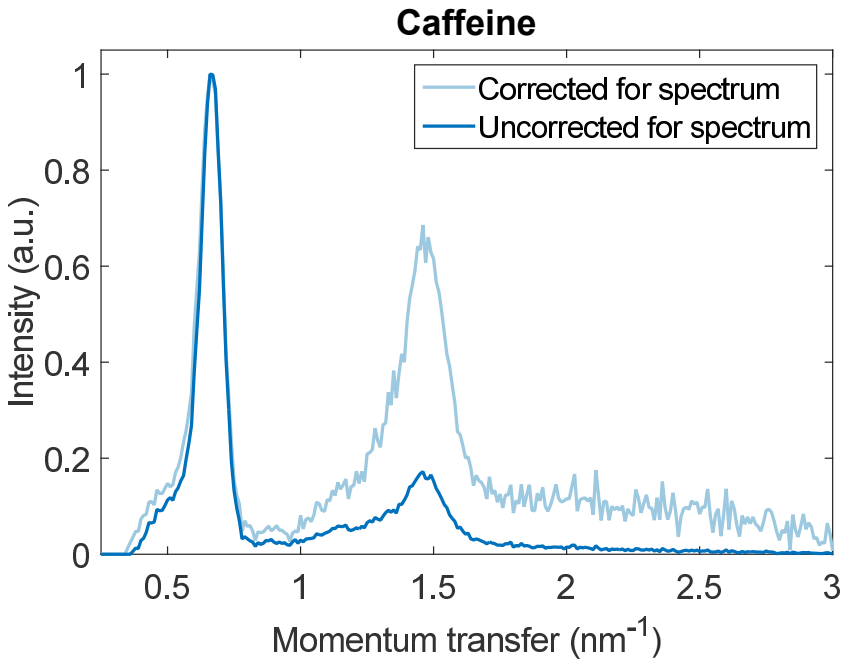

Figure 5. X-ray diffraction patterns for caffeine obtained by converting the pixellated diffraction data into momentum transfer space. Both datasets are background subtracted and corrected for momentum transfer weighting, and the effect of correcting for the X-ray spectrum is shown.

here referred to as peak A and peak B, respectively) are in agreement with those seen in previously published ADXRD data for caffeine [17, 18]. Peak A has a full width at half maximum (FWHM) of 0.09 nm^{-1}, and peak B has a FWHM of 0.17 nm^{-1}. This difference in peak widths is likely due to the larger separation of the unresolved peaks at peak B compared with those at peak A.

The diffraction data for caffeine corrected for background contributions and momentum transfer weighting is shown in Figure 5. Also shown is the result of a normalisation for the X-ray spectrum emitted from the Mini-X source. The output spectrum at 50 kV was directly measured using HEXITEC. When applying the spectral correction, the relative intensities at higher momentum transfer are increased markedly, albeit with an associated increase in statistical noise - due to the drop off of incident photons at the higher energy end of the Bremsstrahlung spectrum. Figure 6 shows the contributions to the overall momentum transfer plot from different energy windows across the range of incident energies. These data illustrate the need to go to energies greater than 15 keV with this detector geometry setup in order to scan a sufficient region of momentum transfer space.

3.2. Hexamine

Diffraction patterns in the form of spots rather than rings indicate the presence of a preferred crystallographic orientation within the sample, or grain sizes which are large

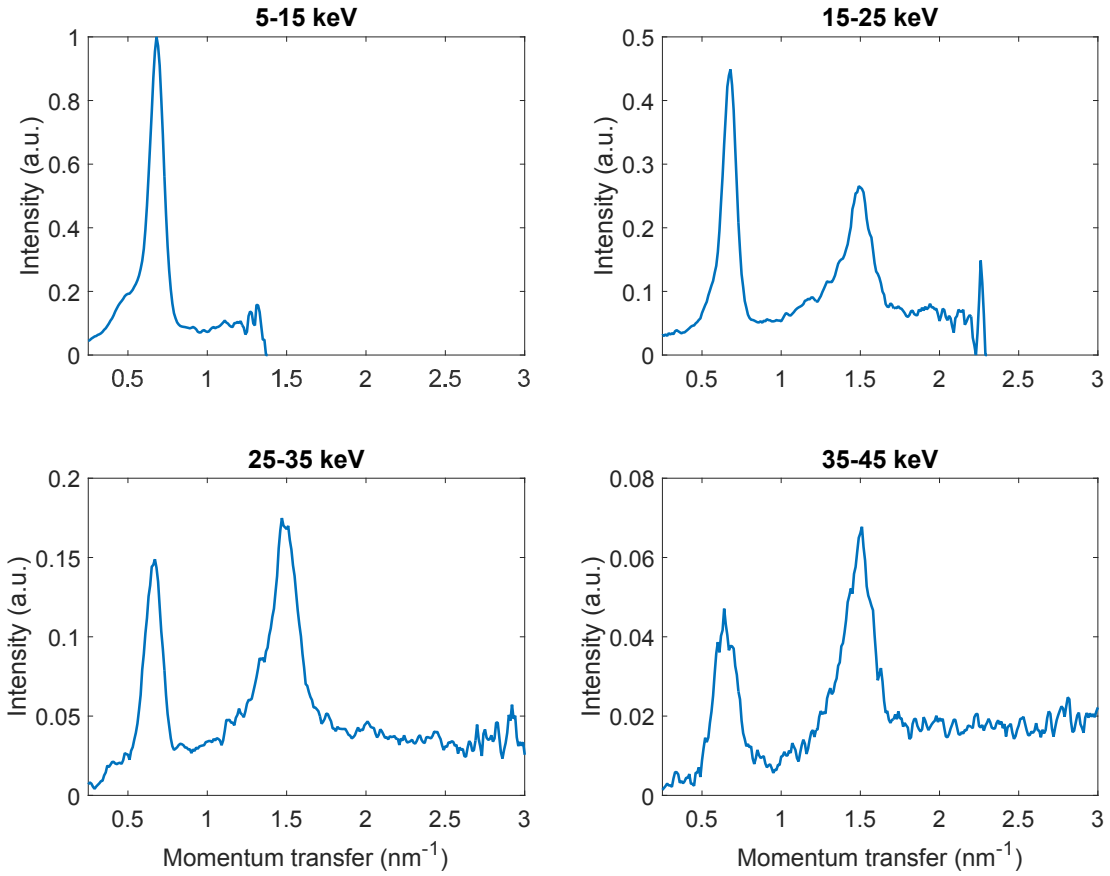

Figure 6. The contribution to the overall momentum transfer spectrum from different energy windows across the range of the incident X-ray spectrum, corrected for background and momentum transfer weighting.

enough such that the incident X-ray beam effectively passes through a limited number of single crystals within the sample. The pixellated diffraction pattern of hexamine shown in Figure 7 is due to the grain size of the sample being comparable with the width of the intersecting X-ray beam (∼1 mm). The ability to detect the diffraction spots from samples such as hexamine over a relatively large area shows a clear advantage of using HEXITEC over small, single element energy-resolving detectors - in the latter case these spots may not be detected due to the detector positioning. The nature of the diffraction images obtained from hexamine in comparison with caffeine demonstrates the potential for grain size determination of an unknown material, which could also be a useful identification metric. In the case of the plastic explosive materials, the pixellated diffraction data show evidence of preferred orientations and/or large grain powders (RDX and/or PETN) being present inside the plastic binding materials for the Semtex and C4 samples (Figure 8).

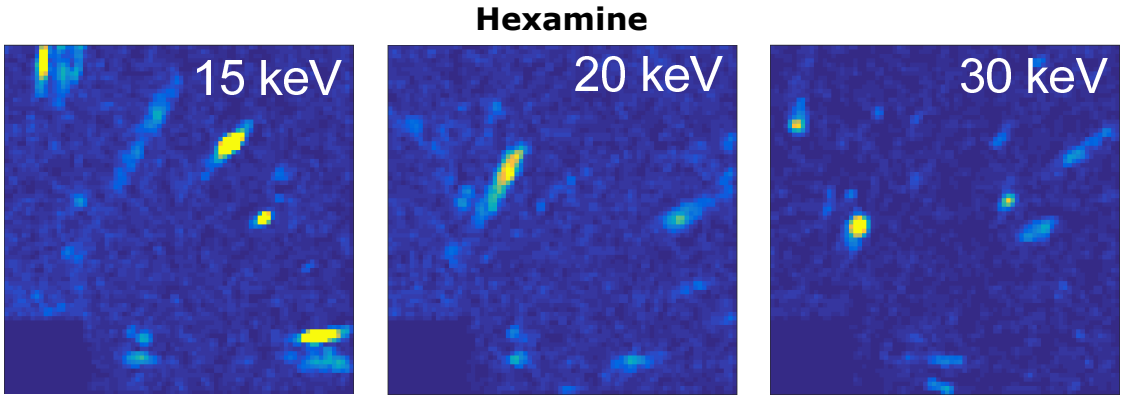

Figure 7. Pixellated X-ray diffraction from hexamine, with X-rays generated at 50 kV and 80 µA, and an acquisition time of 600 s. The energy windows shown have a width of 3 keV.

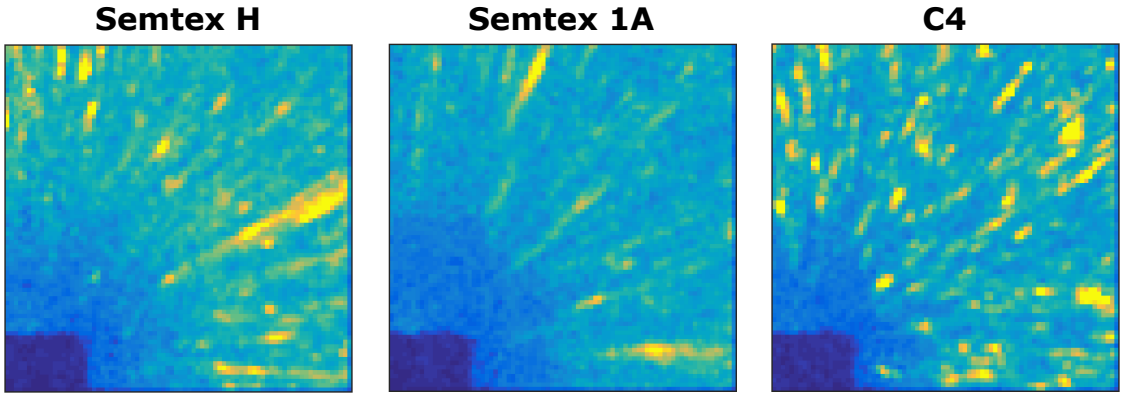

Figure 8. Pixellated diffraction patterns for plastic explosive compounds, summed over all energies.

3.3. Illicit drugs

The compositions of the illicit drug samples are given in Table 1. Note that since the materials with which the drugs were cut had unknown quantities, it is difficult to infer any impact these may have on these diffraction data. There is limited XRD information available on cocaine and diamorphine in the literature, although previous EDXRD studies by Cook *et al.* [19, 20] were used to make a comparison with the data shown here. The diffraction spectrum for diamorphine obtained with the PixD method shows three peaks in intensity at momentum transfers of 0.7, 0.9 and 1.15 nm^{-1} (Figure 9). This result correlates with that found for freebase heroin (of which diamorphine is the active ingredient) by Cook *et al.*

Cocaine in two different forms was also studied using EDXRD by Cook *et al.*, where it was found that the freebase form had a markedly different diffraction spectrum to that of cocaine hydrochloride. The cocaine samples provided for this study were in an unknown form, but by comparison of their diffraction profiles with those shown in the previous EDXRD work they appear to be cocaine hydrochloride, which contains a series

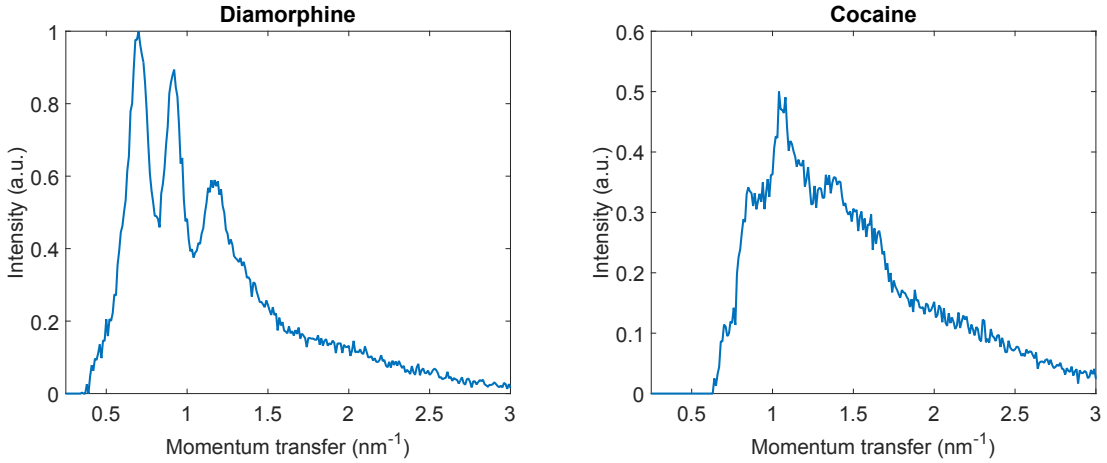

Figure 9. Pixellated diffraction spectra for illicit drug materials, background subtracted and normalised for the momentum transfer weighting in the detector.

of peaks in the momentum transfer range 0.9-1.6 nm^{-1}.

3.4. Aspirin and paracetamol

The observed diffraction profiles for aspirin tablets inside and outside of the blister packaging are given in Figure 10. The features seen in both profiles are similar, with a slightly higher background seen for the aspirin in package data, thought to be due to extra X-ray scatter from the packaging. In order to better understand the nature of the PixD results obtained for aspirin, they were compared with previously acquired high resolution diffraction data of a ground up aspirin tablet taken on synchrotron beamline ID31 at the ESRF, France [21]. The synchrotron data were taken in angular dispersive mode with an X-ray energy of 15.60 keV (wavelength of 0.794 83 Å). An agreement between the PixD and synchrotron data is seen. In particular, the single peak at 0.88 nm^{-1}, the multiple peaks between 1.16 and 1.30 nm^{-1} and the double peak at 1.51 nm^{-1} in the synchrotron data correspond with the three respective main peaks in the pixellated diffraction data.

Paracetamol commonly forms in one of two distinct polymorphs in its pharmaceutical form [22, 23]. A pixellated diffraction measurement was taken on a crushed paracetamol tablet, and the resultant diffraction pattern is shown in Figure 11. These data correspond with previously published ADXRD diffractometer data for the monoclinic Form I polymorph of paracetamol [24, 25].

3.5. Principal component analysis

Principal component analysis (PCA) is a data analysis technique which determines the largest variances between datasets, and can vastly reduce large quantities of data by transforming them into a new space [26, 27]. In this principal component (PC) space, datasets which are similar are grouped in nearby regions, and sets which are different are

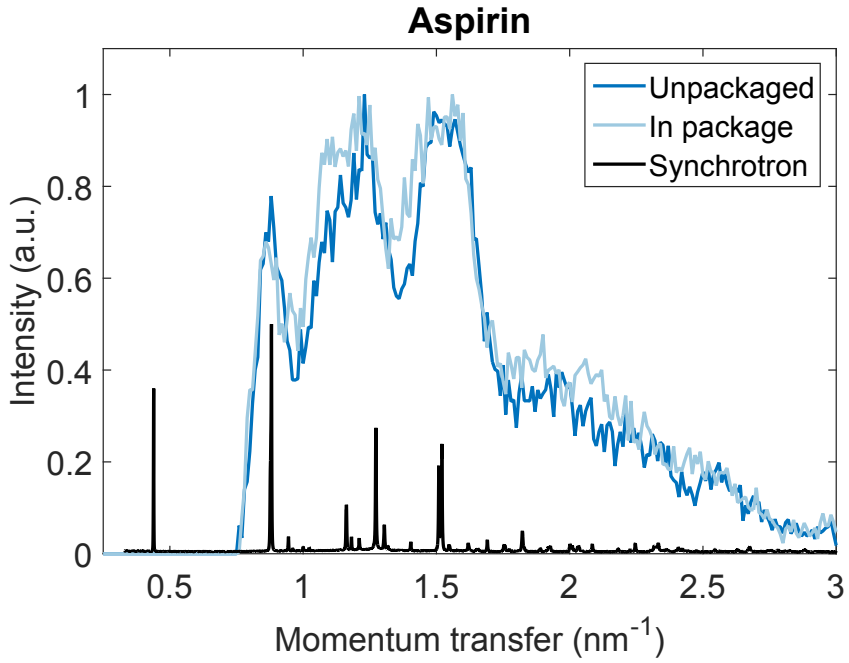

Figure 10. Pixellated diffraction spectra for an aspirin tablet, both inside and outside of its packaging. Data are background subtracted and normalised for the momentum transfer weighting in the detector. For comparison, synchrotron X-ray diffraction data from a ground aspirin tablet is shown, taken at the ID31 beamline, ESRF, France [21].

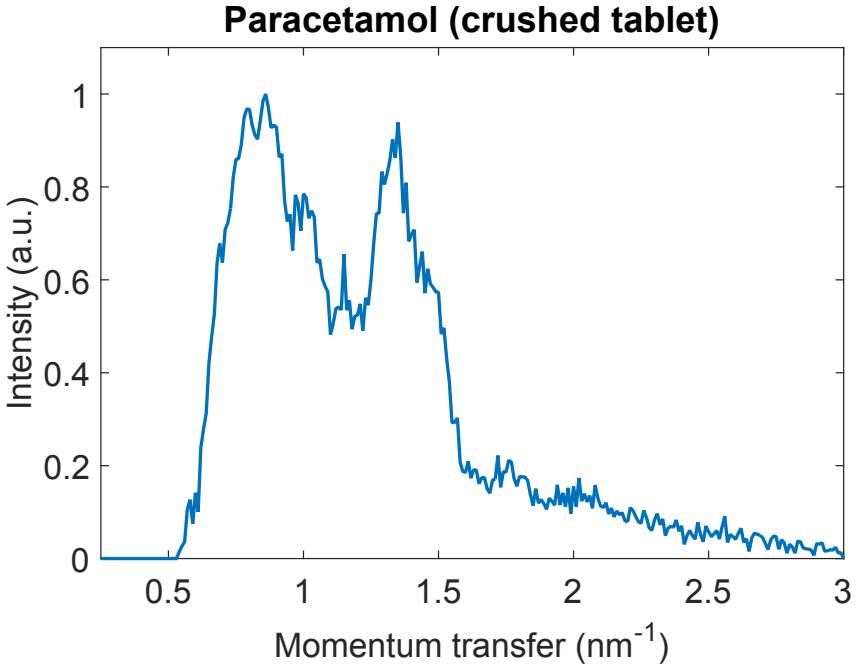

Figure 11. Pixellated diffraction spectra for a crushed paracetamol tablet, background subtracted and normalised for the momentum transfer weighting in the detector.

	Illicit drug quantity	Other materials
Diamorphine 1	73%	Phenobarbitone
Diamorphine 2	69%	Phenobarbitone Caffeine Diazepam
Diamorphine 3	42%	Phenobarbitone Caffeine Diazepam Paracetamol
Cocaine 1	75%	Unknown
Cocaine 2	69%	Unknown

Table 1. Compositions of the illicit drug samples provided by the UK Home Office.

easily separated, making PCA ideal for pattern matching algorithms. The first principal component axis (PC1) describes the largest variance between the datasets. The second axis (PC2) describes the largest variance constrained to be orthogonal to PC1, and so on.

PCA has been shown to work with noisy data [28], and thus it is a useful tool for determining the minimum acceptable acquisition time for the PixD technique using the Mini-X source. PCA was performed on the data after grouping all diffraction spectra into one matrix (different samples in each row, the time normalised intensity at each momentum transfer value in the columns). The result of the analysis was a series of scores for each sample, which can be visualised as their coordinates in PC space. The result of the PCA on the data presented in the previous section, with acquisition times of 5, 10, 60 and 600 seconds is shown in Figure 12. For acquisition times greater than five seconds, there is a clustering of the data points representing each sample. This clustering breaks down when including the data collected for less than five seconds, with points representing these datasets beginning to overlap with other clusters. This can be explained by the noise in these datasets being large enough so as to mask the features which are used by the PCA to differentiate the spectra. In the case of data collected for five or more seconds, the different materials are clearly separable using the first three principal components, and the acquisition times have no significant bearing on the overall position in PC space of each material. For materials identification purposes, this is a very useful result, since discriminant analysis can be used to classify regions in PC space; unidentified materials can then be classified based on which region they fall in to as defined by the discriminant analysis. This approach requires prior knowledge in the form of a library of diffraction spectra of materials to be tested against.

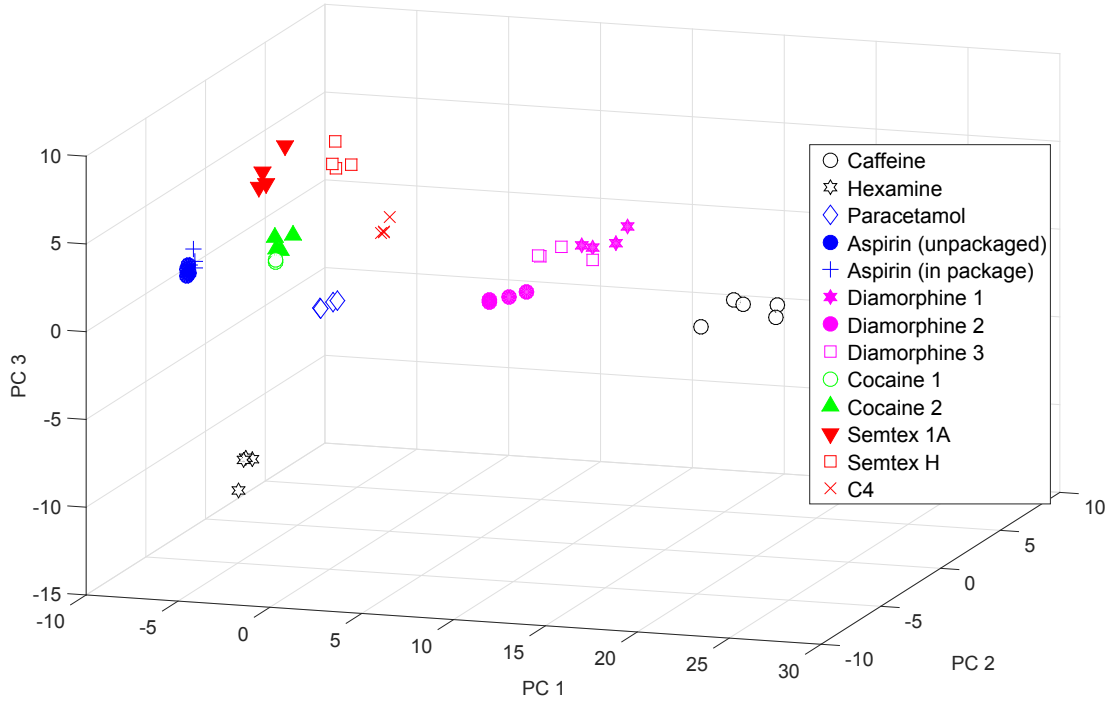

Figure 12. Principal component analysis of the materials studied for this work. The first three principal component axes are shown.

4. Conclusion

It has been demonstrated that the pixellated diffraction technique can be performed with a small-scale X-ray source, showing the potential for translation of the system from a laboratory environment to a portable materials identification system. The ability of X-rays to penetrate through packages - especially the aluminium foil in blister packaging for pharmaceutical tablets - is a clear advantage over existing techniques, and the ability of XRD to probe molecular structure gives a high degree of sample specificity. The HEXITEC detector allows photons of a wide range of energies, and scattered over a range of angles, to be collected simultaneously, giving high counting statistics and allowing as much of the incident and scattered X-rays to be used as possible, without excessive filtration or collimation. The ability to take diffraction images is particularly useful in the case of larger grain crystalline materials or materials with preferred orientations, which give diffraction patterns composed of spots rather than Debye-Scherrer rings. Pixellated diffraction can therefore provide information on the grain size or crystallographic nature of a material, giving further potential identification metrics. If required, the effects due to large grains or preferred orientations can be mitigated by sampling over many different positions of the sample.

For this study, absorption of the X-ray beam was kept to a minimum by using samples thinner than 5 mm. This choice was made for two reasons: to limit the effect of beam attenuation over the energy range available (up to 50 keV), and also to reduce

the loss of angular resolution due to scatter from different depths within the sample [6]. The relatively low maximum current output for the Mini-X tube of 80 µA (at 50 kV) affected the counting statistics of the experiment, and so the minimum counting time required in order to successfully distinguish between different samples. The acquisition time of five seconds reported here is still relatively fast for illicit materials identification, especially when minimal sample preparation is required. The technique of principal component analysis demonstrates that material identification can be achieved through pattern recognition - although a prior library of materials to test for is needed.

5. Acknowledgements

This research was funded under the Innovative Research Call in Explosives and Weapons Detection (2010) initiative, a cross-government programme sponsored by a number of departments and agencies under the UK Government's CONTEST strategy, in partnership with US Department of Homeland Security. The explosives and narcotics samples were provided by the Home Office Centre for Applied Science and Technology. The experiments and handling of these samples were conducted in full compliance with UK laws, rules and regulations.

References

[1] Shell J W 1963 *Journal of Pharmaceutical Sciences* **52** 24–29 ISSN 1520-6017
[2] Peplow D E and Verghese K 1998 *Physics in Medicine and Biology* **43** 2431
[3] Harding G and Schreiber B 1999 *Radiation Physics and Chemistry* **56** 229 – 245 ISSN 0969-806X
[4] Kämpfe B, Luczak F and Michel B 2005 *Particle & Particle Systems Characterization* **22** 391–396 ISSN 1521-4117
[5] O'Flynn D, Reid C B, Christodoulou C, Wilson M D, Veale M C, Seller P, Hills D, Desai H, Wong B and Speller R 2013 *Journal of Instrumentation* **8** P03007
[6] O'Flynn D, Desai H, Reid C B, Christodoulou C, Wilson M D, Veale M C, Seller P, Hills D, Wong B and Speller R D 2013 *Crime Science* **2** 4
[7] Jones L, Seller P, Wilson M and Hardie A 2009 *Nuclear Instruments and Methods in Physics Research Section A: Accelerators, Spectrometers, Detectors and Associated Equipment* **604** 34 – 37 ISSN 0168-9002 Proceedings of the 8th International Conference on Position Sensitive Detectors
[8] Seller P, Bell S, Cernik R J, Christodoulou C, Egan C K, Gaskin J A, Jacques S, Pani S, Ramsey B D, Reid C, Sellin P J, Scuffham J W, Speller R D, Wilson M D and Veale M C 2011 *Journal of Instrumentation* **6** C12009
[9] Veale M C, Kalliopuska J, Pohjonen H, Andersson H, Nenonen S, Seller P and Wilson M D 2012 *Journal of Instrumentation* **7** C01035
[10] Llopart X, Campbell M, Dinapoli R, San Segundo D and Pernigotti E 2002 *Nuclear Science, IEEE Transactions on* **49** 2279–2283 ISSN 0018-9499
[11] Ballabriga R, Campbell M, Heijne E, Llopart X and Tlustos L 2007 *Nuclear Science, IEEE Transactions on* **54** 1824–1829 ISSN 0018-9499
[12] Bellazzini R, Spandre G, Brez A, Minuti M, Pinchera M and Mozzo P 2013 *Journal of Instrumentation* **8** C02028
[13] Romano A, Pacella D, Claps G, Causa F and Gabellieri L 2015 *Journal of Instrumentation* **10** C02046

[14] Vincenzi A, de Ruvo P, Delogu P, Bellazzini R, Brez A, Minuti M, Pinchera M and Spandre G 2015 *Journal of Instrumentation* **10** C04010
[15] Newton P N, Green M D, Fernndez F M, Day N P and White N J 2006 *The Lancet Infectious Diseases* **6** 602 – 613 ISSN 1473-3099
[16] Dégardin K, Roggo Y and Margot P 2014 *Journal of Pharmaceutical and Biomedical Analysis* **87** 167 – 175 ISSN 0731-7085 review Papers on Pharmaceutical and Biomedical Analysis 2013
[17] Phadnis N V, Cavatur R K and Suryanarayanan R 1997 *Journal of Pharmaceutical and Biomedical Analysis* **15** 929 – 943 ISSN 0731-7085
[18] Lehmann C and Stowasser F 2007 *Chemistry A European Journal* **13** 2908–2911 ISSN 1521-3765
[19] Cook E, Fong R, Horrocks J, Wilkinson D and Speller R 2007 *Applied Radiation and Isotopes* **65** 959 – 967 ISSN 0969-8043
[20] Cook E, Pani S, George L, Hardwick S, Horrocks J and Speller R 2009 *IEEE Transactions on Nuclear Science* **56** 1459 –1464 ISSN 0018-9499
[21] Reproduced with permission from A. Fitch at the ESRF `http://www.iucr.org/resources/commissions/powder-diffraction/projects/organic-datasets`
[22] Nichols G and Frampton C S 1998 *Journal of Pharmaceutical Sciences* **87** 684–693 ISSN 1520-6017
[23] Espeau P, Colin R, Tamarit J L, Perrin M A, Gauchi J P and Leveiller F 2005 *Journal of Pharmaceutical Sciences* **94** 524–539 ISSN 1520-6017
[24] Pecharsky V K and Zavalij P Y 2009 *Fundamentals of Powder Diffraction and Structural Characterization of Materials* (Springer US) ISBN 978-0-387-09578-3
[25] Perrin M A, Neumann M A, Elmaleh H and Zaske L 2009 *Chem. Commun.* (22) 3181–3183
[26] Lee D D and Seung H S 1999 *Nature* **401** 788–791 ISSN 0028-0836
[27] Theodorakou C and Farquharson M J 2009 *Physics in Medicine and Biology* **54** 4945
[28] Luggar R D, Farquharson M J, Horrocks J A and Lacey R J 1998 *X-Ray Spectrometry* **27** 87–94 ISSN 1097-4539